Journal of Sound and Vibration (1998) **209**(3), 473–492

STRONGLY NON-LINEAR OSCILLATIONS OF WINDING MACHINES, PART I: MODE-LOCKING MOTION AND ROUTES TO CHAOS

Y. KANG AND Y.-P. CHANG

Department of Mechanical Engineering, Chung Yuan Christian University, Taiwan, R.O.C.

AND

S.-C. JEN

Department of Mechanical Engineering, Sze Hai Institute of Technology and Commerce, Taiwan, R.O.C.

(*Received* 10 *June* 1996, *and in final form* 28 *July* 1997)

This study investigates the dynamics of a single-degree-of-freedom (SDOF) wire in a winding machine. This system has piecewise-linear stiffness and is subjected to a forcing excitation due to imbalance and a parametric excitation due to tension. The frequencies of both parametric and forcing excitations are not equal or do not have a ratio of two simple integers. Using the fourth order Runge–Kutta method and introducing a *J*-integral, this strongly non-linear system can be estimated for various parameters. Then, the mode-locking motions, main resonant intervals, and subharmonic modes can be found. Also, all possible combined subharmonics and superharmonic motions and routes to chaos are observed by *J*-bifurcation illustrations with the assistance of Poincaré maps, phase portraits, response waveforms, frequency spectra and Lyapunov exponents. Thus, the physical illustrations of such a system can provide stabilization by appropriate design parameters.

1. INTRODUCTION

The strongly non-linear dynamics of piecewise-linear mechanical systems is an important practical problem, because such systems are commonly used in many engineering fields. Piecewise-linear systems containing components with clearance are either designed and assembled unavoidably, or due to wear, experience intermittent motion from contact with a separation from other components, or connect through a backlash. These systems exhibit phenomena such as multiple solution regimes, and superharmonic, subharmonic and quasi-periodic and chaotic solutions.

The conventional methods for analyzing piecewise-linear systems which are subjected to an harmonic force can be categorized into the following solution techniques. (i) Padmanabhan and Singh [1] have adapted an analytical method of the parametric continuation scheme, based on the shooting method. Although the occurrence of a period-doubling bifurcation determined by the eigenvalues of period two was solved, the periodic solutions were scarcely obtained. (ii) Choi and Noah [2, 3], Kim and Noah [4], Lau and Zhang [5] and Narayanan and Sekar [6] used the harmonic balance method to determine the coefficients of solutions directly or iteratively; however, these coefficients corresponding to the synchronous or multiple forcing frequency do not seem to converge easily to finite terms. Furthermore, the influence of initial conditions on steady state

0022–460X/98/030473 + 20 $25.00/0/sv971250

solutions was no longer unambiguous. Neither were these solutions identical to the ones for the original equations of motion; consequently, the solutions were only approximate. (iii) Mahfouz and Badrakhan [7, 8] used the numerical integration method to solve two non-linear systems having only forcing excitations with harmonic frequency and obtained harmonic, subharmonic and chaotic motions for various parameters. Oks *et al*. [9] investigated the suppression phenomena of resonant oscillations in these strongly non-linear SDOF systems with parametric and forcing frequencies. The resonance and non-resonance regions were determined; however, the details of the periodic, subharmonic and chaotic motions have not been observed.

This study investigates the dynamics of a winding machine with piecewise-linear stiffness, which is an SDOF system subjected to a parametric excitation and a forcing excitation with a non-multiple frequency ratio. This system is described by a second order differential equation and solved by the fourth order Runge–Kutta method to determine the stationary J-integral solutions for various parameters. J-integral bifurcation can be analyzed by means of Poincaré maps, frequency spectra, response waveforms, phase portraits and Lyapunov exponents to distinguish the jump phenomenon, frequency-locking, routes to chaos and resonance/non-resonance due to initial conditions.

2. EQUATIONS OF MOTION

In a winding machine, one-mode oscillations of a stretched string, as shown in Figure 1, can be governed by the equation [9]

$$m\frac{\mathrm{d}^2y}{\mathrm{d}t^2} + c\frac{\mathrm{d}y}{\mathrm{d}t} + k_1(1 - \mu_2 \sin(\omega_2 t))y + F(y) = p \sin(\omega_1 t), \tag{1}$$

in which the piecewise-linear restoring force $F(y)$ is generated by a clearance ε and is given by

$$F(y) = \begin{cases} 0 & \text{for } |y| \leqslant \varepsilon, \\ (k_2 - k_1)(y - \varepsilon \operatorname{sgn} y) & \text{for } |y| > \varepsilon, \quad k_1 < k_2, \end{cases} \tag{2}$$

where m is the lump mass of a winding wire, c is the linear damping coefficient, k_1 and k_2 are the wire stiffness and the restoring stiffness, respectively, ω_1 and ω_2 are the forcing and the parametric frequencies, respectively, and p and μ_2 are the amplitudes of the forcing and the parametric excitations, respectively. The parametric excitation is due to the tension

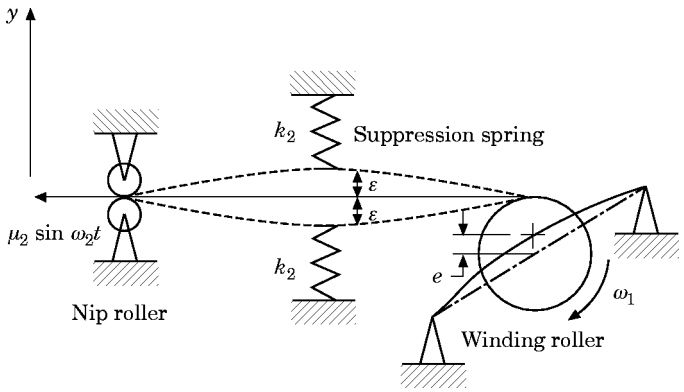

Figure 1. A model of a winding machine.

TABLE 1

System parameters for the figures

	v_1	v_2	μ_1	μ_2	k	γ	$x(0)$	$\dot{x}(0)$
Figure 2	1·23	3·0	0·25	0·17	7·0	(a) 0·15	− 1·8	0
						(b) 0·1	−2·0	0
						(c) 0·086	−1·8	0
						(d) 0·07	0	0
						(e) 0·07	−0·75	0
Figure 3	1·23	3·0	0·25	0·17	7·0	0·07	−0·75	0
Figure 4	1·23	3·0	0·25	0·17	7·0	0·06–0·20 Step = 0·0002	−2·5–0·0 Step = 0·05	0
Figure 5	1·23	3·0	0·1–0·5 Step = 0·001	0·18	7·0	1/15	−2·5–0·0 Step = 0·05	0
Figure 6	1·23	3·0	(a) 0·1	0·18	7·0	1/15	−1·2	0
			(b) 0·163				−2·0	0
			(c) 0·199				−1·4	0
			(d) 0·204				−2·1	0
			(e) 0·206				−2·0	0
			(f) 0·136				−1·45	0
			(g) 0·205				−1·65	0
Figure 7	1·23	3·0	(a) 0·349	0·18	7·0	1/15	−2·1	0
			(b) 0·348				−0·9	0
			(c) 0·375				−2·1	0
			(d) 0·375				−2·45	0
			(e) 0·298				−1·25	0
Figures 8 and 9	1·23	3·0	0·1–0·5 Step = 0·001	0·18	7·0	1/15	Resonant region	0
Figure 10	1·23	3·0	0·25	0·17	7·0	(a) 0·15	−2·5–2·5 Step = 0·05	−5–5 Step = 0·1
						(b) 0·1		
						(c) 0·07		
Figure 11	1·23	3·0	0·1–0·5 Step = 0·001	0·15	7·0	1/15	−2·5–0·0 Step = 0·05	0
Figure 12	1·23	3·0	0·145	0·15	7·0	1/15	−2·5–2·5 Step = 0·05	−5–5 Step = 0·1

of the string, and the forcing excitation is caused by the whirling motion of a winding roller installed at the right end.

Substitution of the following non-dimensional variables,

$$x = y/\varepsilon, \qquad \tau = \omega_0 t, \qquad \omega_0 = \sqrt{k_1/m}, \qquad \mu_1 = p/(k_1 \varepsilon), \qquad v_1 = \omega_1/\omega_0,$$
$$v_2 = \omega_2/\omega_0, \qquad \gamma = c/(m\omega_0), \qquad k = (k_2 - k_1)/k_1, \tag{3}$$

into equations (1) and (2) gives

$$\ddot{x} + \gamma\dot{x} + (1 - \mu_2 \sin(v_2 \tau))x + f(x) = \mu_1 \sin v_1 \tau, \tag{4}$$

where

$$f(x) = \begin{cases} 0 & \text{for } |x| \leqslant 1, \\ k(x - \operatorname{sgn} x) & \text{for } |x| > 1, \end{cases} \tag{5}$$

and the superscript dot denotes differentiation with respect to τ.

Since this equation has a strong non-linear restoring force and the forcing frequency has a non-multiple value via the parametric frequency, there has been no analytical method of solution. Thus, the fourth order Runge–Kutta method is utilized, for various values of system parameters within the following ranges:

$$1 \leqslant k \leqslant 10, \qquad 0 < \mu_2 \leqslant 0{\cdot}5, \qquad 0{\cdot}02 \leqslant \gamma \leqslant 0{\cdot}2, \qquad 0 < \mu_1 \leqslant 1, \qquad 0{\cdot}5 \leqslant \nu_1 < 2.$$

The initial conditions of the non-dimensional displacement are from $-2{\cdot}5$ to $2{\cdot}5$, and the non-dimensional velocity from $-5{\cdot}0$ to $5{\cdot}0$ is considered. Values of these parameters with respect to Figures 2–12 are listed in Table 1. The value N is chosen in the range 200–600

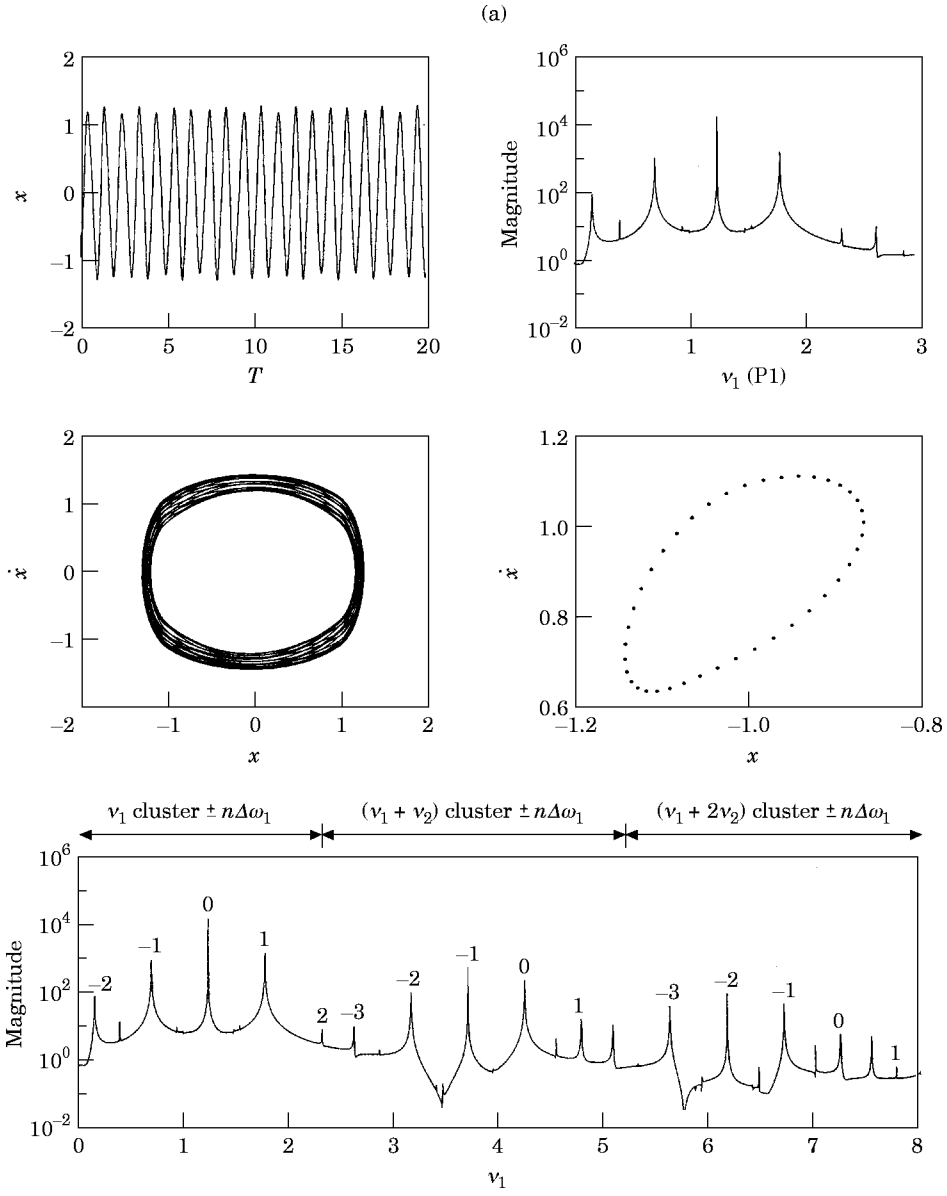

Figure 2a.

(b)

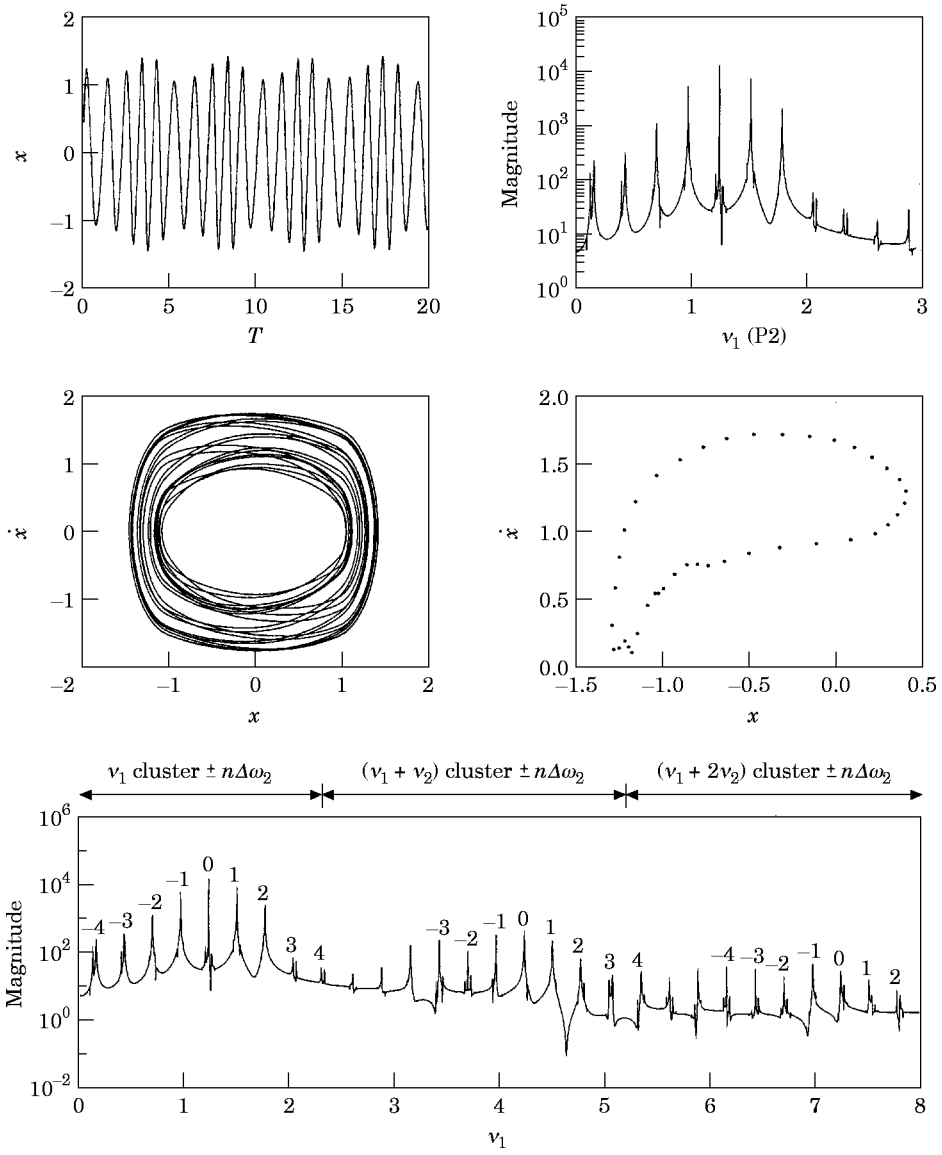

Figure 2b.

for the time interval $\Delta\tau = 2\pi/(\nu_1 N)$ in the numerical integration. The first forcing periods, which have long terms, were not recorded in order to avoid transient solutions. Both the frequency spectrum and the phase portrait are determined for 100 forcing periods. Poincaré maps are obtained by sampling the stationary solutions over 200 points $(x, \dot{x})$ for one forcing period $(T = 2\pi/\nu_1)$.

3. FREQUENCY-LOCKING AND QUASI-PERIODIC MOTIONS

A winding wire system is characterized by two frequencies which belong to forcing and parametric excitations. A type of quasi-periodic motion can occur, because this system has

two different frequencies associated with it; that is, it can be analyzed with regard to two independent periodic motions. The pattern of points on a Poincaré map looks like a dependence on the numerical relationship between the two frequencies. If the ratio of the two frequencies can be expressed as the ratio of two integers (that is, as a "rational fraction"), then the Poincaré section will consist of a finite number of points. This type of motion is often called frequency-locked—or mode-locking or phase-locking—motion, because one of the frequencies is locked, often over a finite control parameter range, as a multiple integer of the other.

If the frequency ratio is irrational, the points on a Poincaré map eventually fill a continuous curve in the Poincaré plane, and the motion is said to be quasi-periodic because

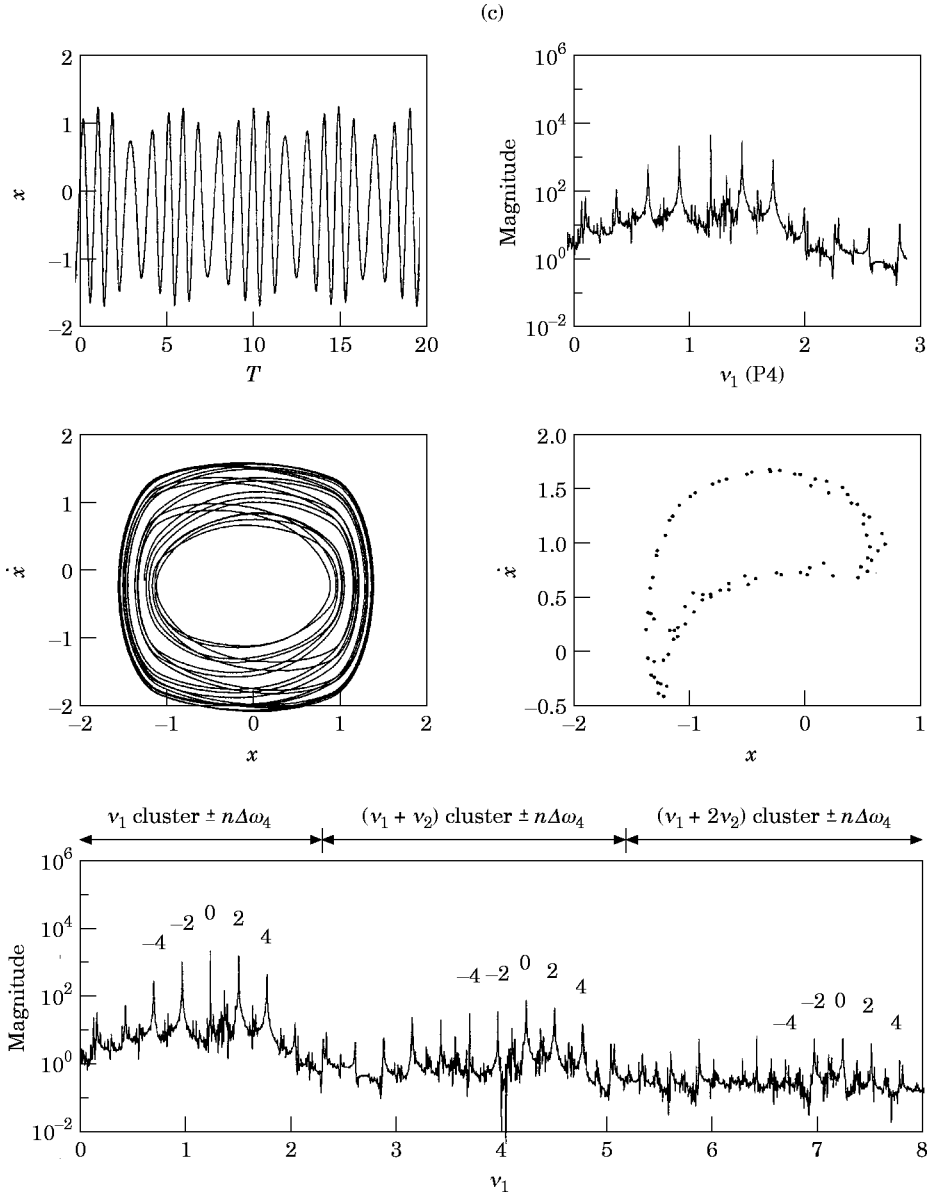

Figure 2c.

(d)

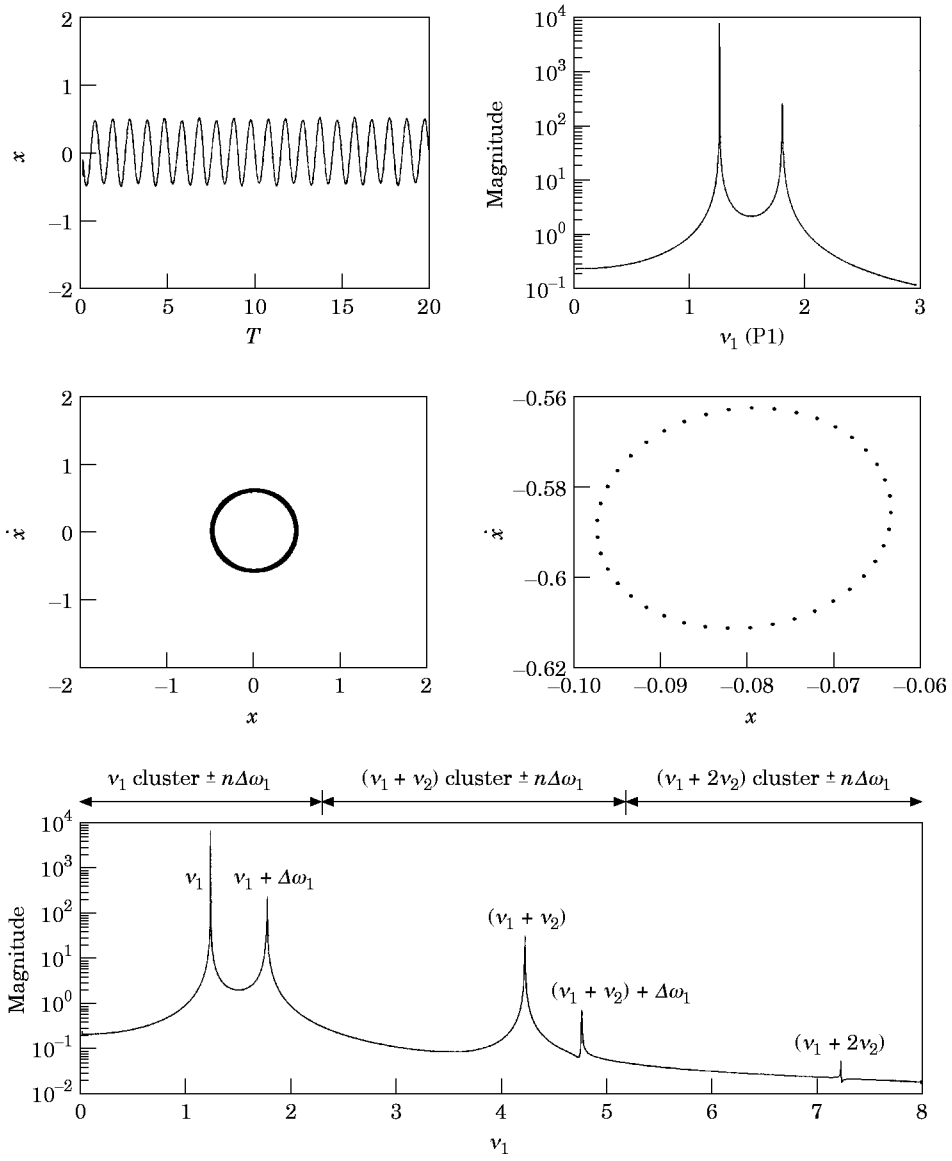

Figure 2d.

the motion never exactly repeats itself. However, the motion is not chaotic; rather, it is composed of two or more periodic components, the presence of which can be determined by measuring the frequency spectrum of motion. In order to detect the difference between quasi-periodic and chaotic motions, the Lyapunov exponents are calculated by using the algorithm devised by Wolf *et al*. [10]. The calculated value of the most positive Lyapunov exponent when the system has chaotic behavior is plotted as a function of the total average time, measured in units of the forcing period. A winding wire system has parameters of $\nu_1 = 1{\cdot}23$, $\nu_2 = 3$, $k = 7$, $\mu_1 = 0{\cdot}25$, $\mu_2 = 0{\cdot}17$ and $\gamma = 0{\cdot}07$, with various initial conditions governed by equations (4) and (5). In Figures 2(a)–2(e) are shown the response waveforms, frequency spectra, phase portraits and Poincaré maps for selecting damping at $\gamma = 0{\cdot}15$,

0·1, 0·086 and 0·07 for this system, respectively. As the frequency ratio $\nu_2/\nu_1 = 100/41$, the stationary responses of the resonant motion are a limit cycle around point (0, 0) and the orbits enlarge monotonously as the damping coefficient γ decreases. The non-resonant motion is shown in Figure 2(d). These figures exhibit frequency-locking motions, which can be observed by 41 Poincaré map points.

As the damping is reduced, the coupling between the two frequencies increases and results in increasing numbers of frequency peaks, which spread throughout the frequency

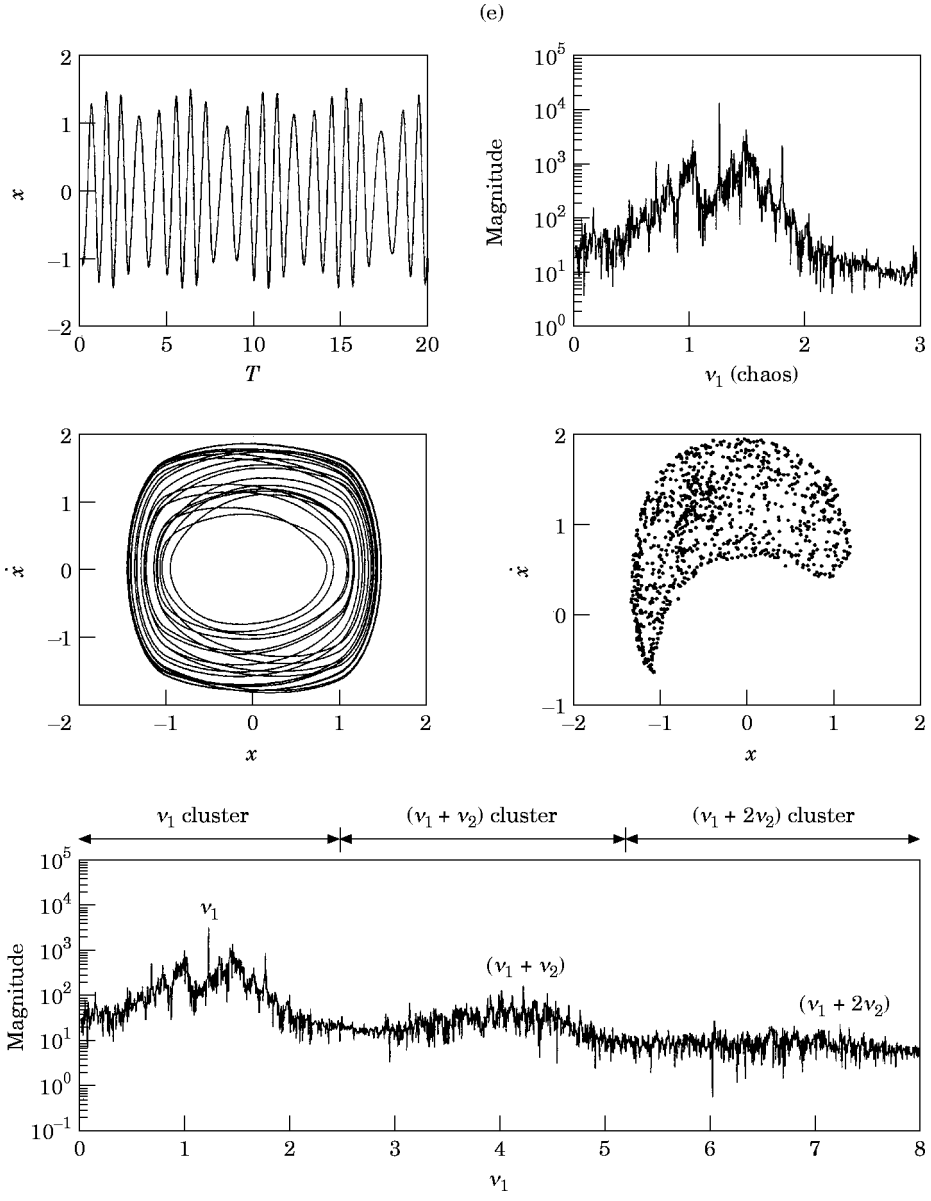

Figure 2e.

Figure 2. Response waveforms (upper left), frequency spectra (upper right), phase portraits (middle left) and Poincaré maps (middle right), and the extent of the long-term frequency spectra (bottom). (a) $\gamma = 0{\cdot}15$ (P1); (b) $\gamma = 0{\cdot}1$ (P2); (c) $\gamma = 0{\cdot}086$ (P4); (d) $\gamma = 0{\cdot}07$ (P1); (e) $\gamma = 0{\cdot}07$ (chaos).

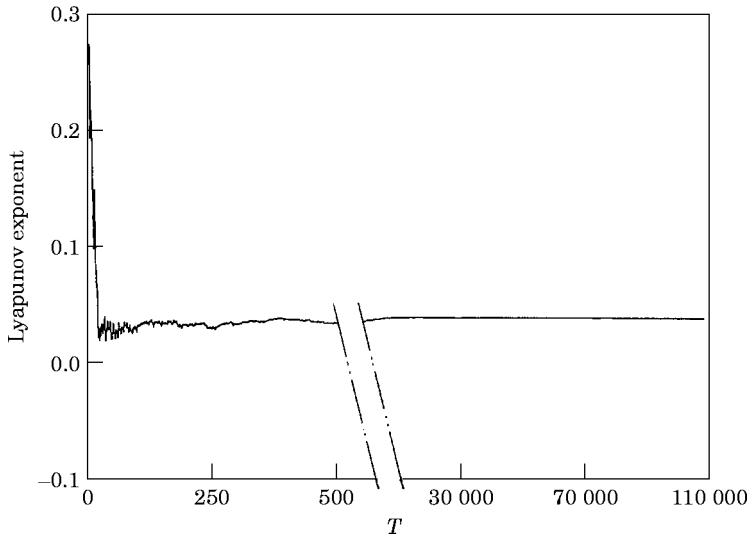

Figure 3. The Lyapunov exponent versus time from Figure 2(e).

spectrum. Figure 2(e) is for $\gamma = 0{\cdot}07$ and $x(0) = -0{\cdot}75$, with other identical parameters, the frequency spectrum of which is random-like. The Lyapunov exponent is determined as shown in Figure 3, where the occurrence of chaotic motion is illustrated.

The frequency components of a period n motion contain a combination of v_1, v_2, the superharmonic v_2, and the subharmonic combination of v_2 and v_1, when it is a mode-locking motion. In the present cases, the parametric and forcing frequencies induce combinations of resonances. The frequency spectrum diagrams in Figures 2(a)–(e) show all of the peak frequencies, which can be described by

$$f_p = (n_1 v_2 + v_1) \pm n_2 \Delta\omega_n \tag{6}$$

where $\Delta\omega_n = |v_2 - 2v_1|/n$, with n an integer, and $n_1, n_2 = 0, 1, 2, \ldots$.

Thus these motions are combinations of the n_1th superharmonic components of v_2, the (n_2/n)th subharmonic components of $v_2 - 2v_1$, and the harmonic components of v_1. One may denote these motions by period n or Pn, because of the corresponding number of peak frequencies in each cluster.

4. BIFURCATION OF J-INTEGRAL

The probability density function and the r.m.s. response are appropriate methods for the analysis of chaos, as shown in references [11, 12]. An effective integral of the response waveforms have been verified as a method of determining whether or not a transient solution leads to one or the other steady solutions [13]. This integral, monitored on the computer, is utilized in this study as shown:

$$J = \int_0^{2\pi/v_1} [\dot{x}(\tau)]^2 \, \mathrm{d}\tau. \tag{7}$$

From a computer analysis with various initial conditions, the steady state solutions of this integral can be obtained. The initial conditions play an important role in determining the resonance or non-resonance, and the system shows multiple solutions. In real systems

the actual disturbances cannot always be expressed in terms of the initial conditions. In general, the calculation of the J-integral for various initial conditions gives the number of values that can correspond to the number of frequencies about the stationary response. The large amplitudes should be distinguished from those having small amplitudes, which determine the occurrences of resonance or non-resonance. The bifurcation of the J-integral is composed of two cascades for which the upper is resonant oscillation and the lower is non-resonant oscillation.

In Figure 4 is shown the bifurcation of the J-integral versus the damping parameter for the same system as in Figure 2. A period-doubling cascade leads to chaotic motions. For the damping values $\gamma = 0{\cdot}15$, $0{\cdot}1$ and $0{\cdot}086$ shown in Figures 2(a), 2(b) and 2(c), respectively, the large J-integrals are period one, period two and period four motions.

In the range $0{\cdot}1764 < \gamma < 0{\cdot}2$, only a small J-integral cascade can be obtained for all initial conditions and this non-resonance is a period one motion. As the damping coefficients γ decrease, a jump phenomenon occurs at $\gamma = 0{\cdot}1764$. For these damping values the initial conditions determine which resonance or non-resonance appears. After a further decrease in the damping parameter γ, period two and period four motions occur at the values of $\gamma = 0{\cdot}1276$ and $\gamma = 0{\cdot}0882$, respectively.

In another example, the winding wire system has parameters of $v_1 = 1{\cdot}23$, $v_2 = 3$, $k = 7$, $\mu_2 = 0{\cdot}18$ and $\gamma = 1/15$. The bifurcations of the J-integral versus the forcing amplitude μ_1, having values from $0{\cdot}1$ to $0{\cdot}5$, are shown in Figure 5. The resonance due to a large J-integral exists among the regions except from $\mu_1 = 0{\cdot}207$ to $0{\cdot}249$; however, non-resonance due to a small J-integral exists from $\mu_1 = 0{\cdot}1$ to $0{\cdot}425$. When μ_1 is increased from $0{\cdot}1$ to $0{\cdot}207$, the resonance cascade shows that the number of J values increases from one, two, four and eight to larger numbers. Then the irregular motions occur during a very narrow range of μ_1. In an inverse direction when μ_1 is decreasing from $0{\cdot}5$ to $0{\cdot}349$, the resonance cascade shows that the numbers of J values change from one to two, and then

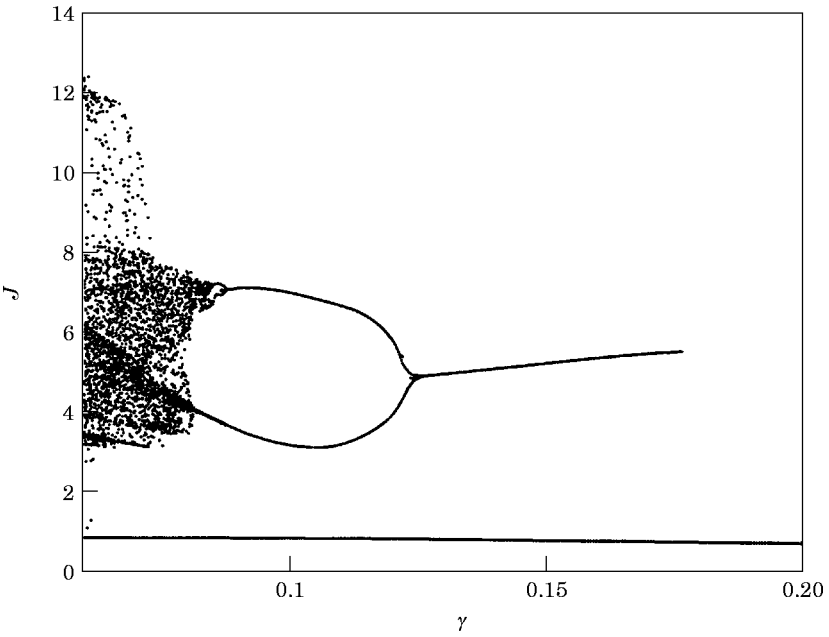

Figure 4. Bifurcation of the integral J (J–γ); $k = 7$, $\mu_2 = 0{\cdot}17$, $\mu_1 = 0{\cdot}25$, $v_1 = 1{\cdot}23$.

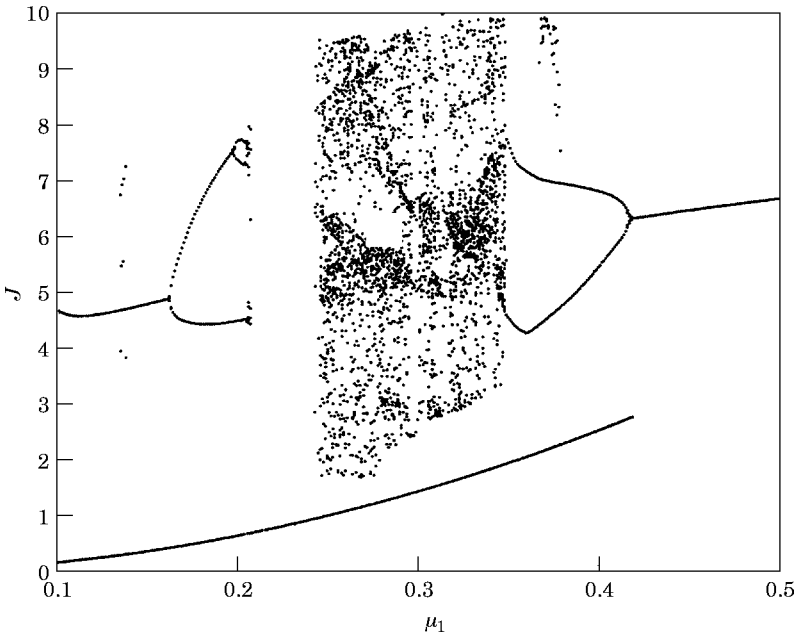

Figure 5. Bifurcation of the integral J (J–μ_1); $k = 7$, $\mu_2 = 0{\cdot}18$, $\gamma = 1/15$, $\nu_1 = 1{\cdot}23$.

immediately to a large number, and the irregular motions occur between $\mu_1 = 0{\cdot}249$ and $\mu_1 = 0{\cdot}349$.

Poincaré maps and frequency spectra for selected values of $\mu_1 = 0{\cdot}1$, $0{\cdot}163$, $0{\cdot}199$, $0{\cdot}204$ and $0{\cdot}206$, respectively, for period one with large amplitude, period two, period four, period eight, and period one with small amplitude motions, are shown in Figures 6(a)–6(e), respectively. When $\mu_1 \simeq 0{\cdot}136$, the map indicates irregular points, due to a period three motion, as shown in Figure 6(f). This period-doubling route leads to chaos at $\mu_1 = 0{\cdot}205$, as shown in Figure 6(g).

When μ_1 decreases from $0{\cdot}5$ to $0{\cdot}25$, the resonance map exhibits period one and period two with a large number of J-integrals. Suddenly, chaotic motion occurs, when $\mu_1 = 0{\cdot}349$ to $\mu_1 = 0{\cdot}348$, as shown in Figures 7(a) and 7(b). When $\mu_1 = 0{\cdot}375$, in this case the three motions P1 (small amplitude), P2 and chaos coexist. In Figures 7(c) and 7(d) are shown the resonant motion for $x(0) = -2{\cdot}1$ and $x(0) = -2{\cdot}45$ respectively. For the forced amplitude $\mu_1 = 0{\cdot}298$ a narrow window of period seven motion appears. Since the frequency ratio $\nu_2/\nu_1 = 100/41$, the Poincaré section of this mode-locking motion has 287 (41×7) points, as shown in Figure 7(e).

The variation of the largest Lyapunov exponent versus μ_1 for a 200 000 forcing period is illustrated in Figure 8. The occurrence of positive values between $0{\cdot}249 < \mu_1 < 0{\cdot}349$, $\mu_1 \simeq 0{\cdot}205$ and $\mu_1 \simeq 0{\cdot}375$ indicates that chaotic motions exist. Within this chaotic window, a narrow periodic window appears. Through signs of Lyapunov exponents [14] ranging from $(0, -, -)$ to $(+, 0, -)$, the large limit cycle solutions undergo a period-doubling bifurcation. Then, the resulting limit cycle undergoes Hopf bifurcation, resulting in a cascade period-doubling, and eventually breaking down into chaos. However, the periodic behavior is interrupted by bursts of chaotic behavior, which can be called period-doubling intermittency.

In the case of some parameters, by picking up J-integral, one can plot J versus the parameter, so that the diagram may appear similar to the bifurcation diagram

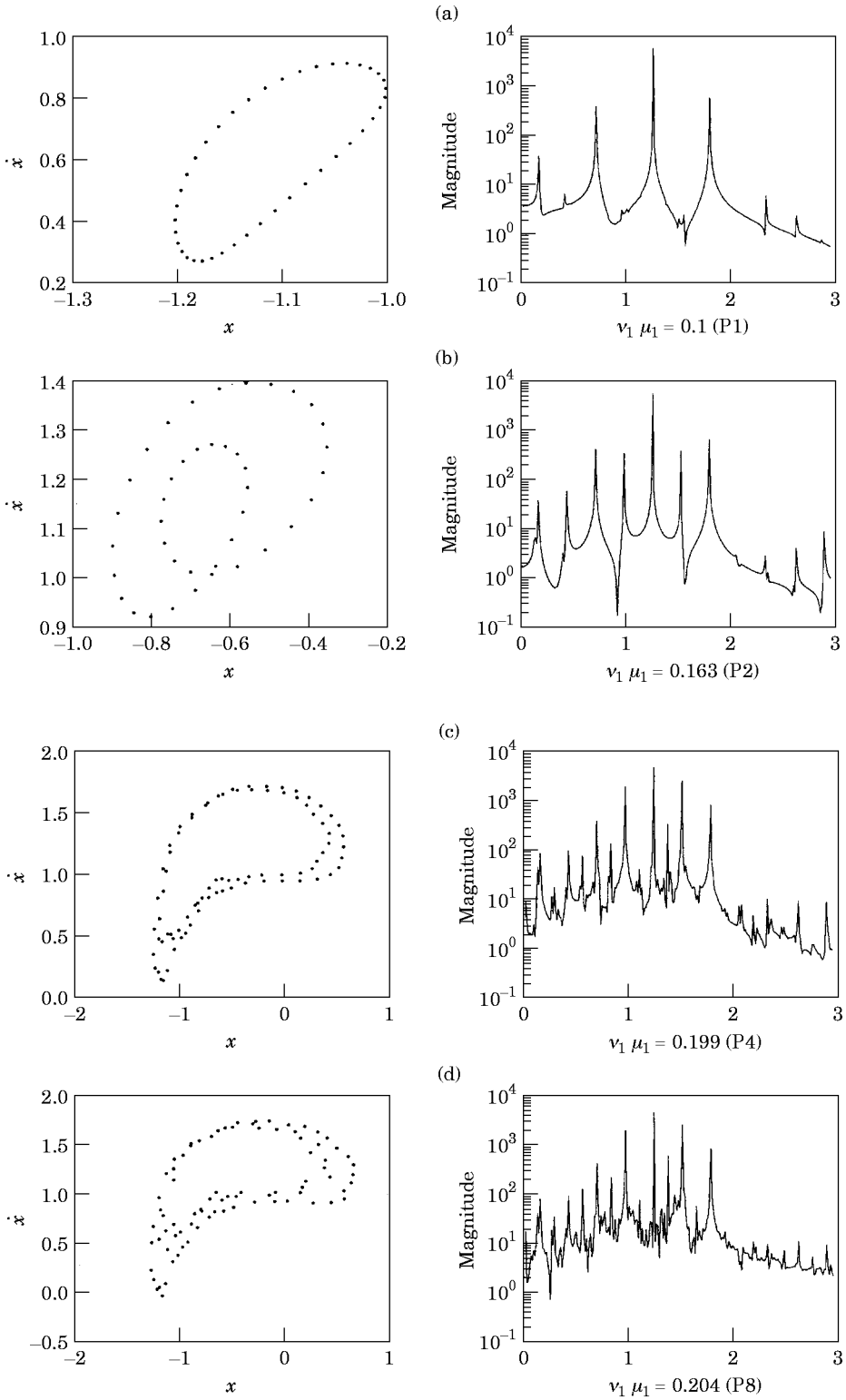
(a)
1.0
0.8
0.6
0.4
0.2
$\dot{x}$
−1.3
−1.2
−1.1
−1.0
x
Magnitude
10^4
10^3
10^2
10^1
10^0
10^{-1}
0
1
2
3
$\nu_1\ \mu_1 = 0.1$ (P1)
(b)
1.4
1.3
1.2
1.1
1.0
0.9
−1.0
−0.8
−0.6
−0.4
−0.2
$\nu_1\ \mu_1 = 0.163$ (P2)
(c)
2.0
1.5
1.0
0.5
0.0
−2
−1
0
1
$\nu_1\ \mu_1 = 0.199$ (P4)
(d)
−0.5
$\nu_1\ \mu_1 = 0.204$ (P8)

Figure 6a-d.

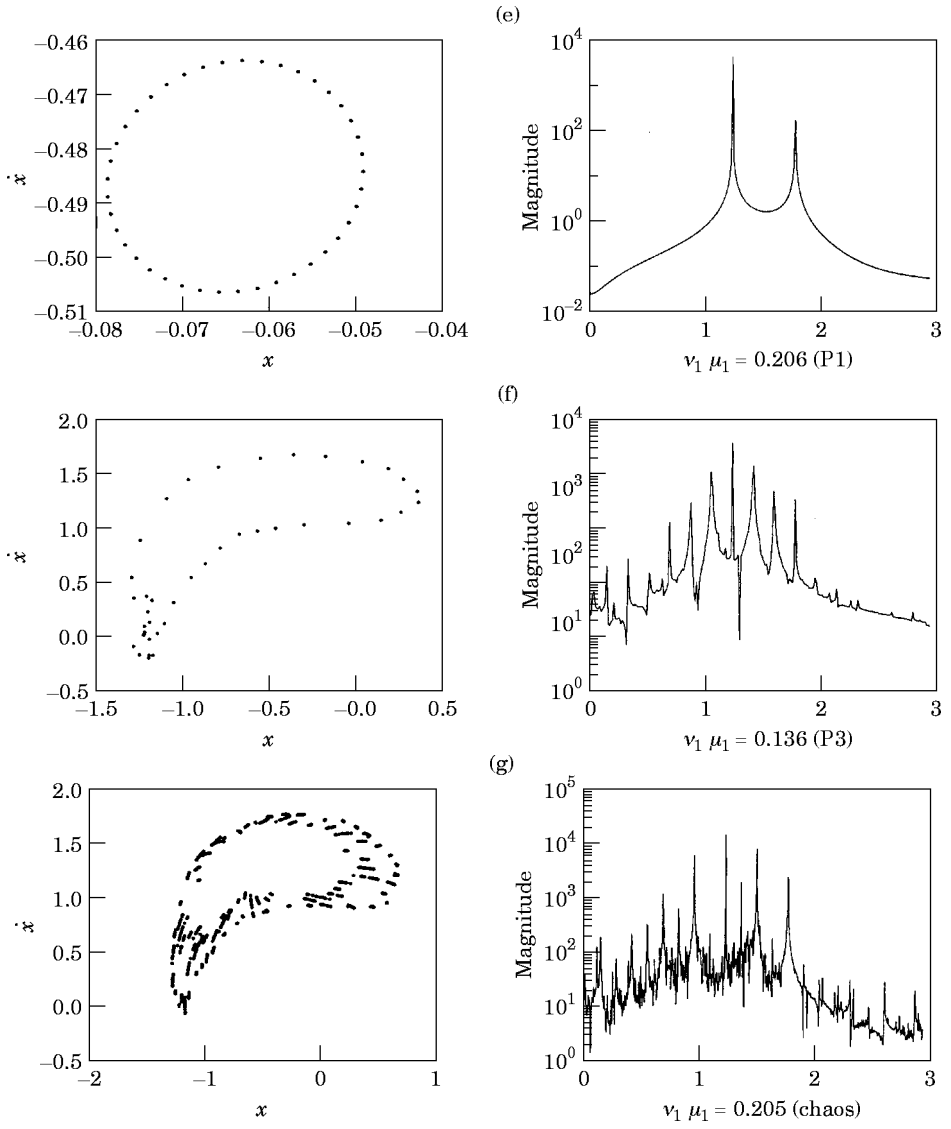

Figure 6e-g.

Figure 6. Poincaré maps (left) and frequency spectra (right). (a) $\mu_1 = 0{\cdot}1$ (P1); (b) $\mu_1 = 0{\cdot}163$ (P2); (c) $\mu_1 = 0{\cdot}199$ (P4); (d) $\mu_1 = 0{\cdot}204$ (P8); (e) $\mu_1 = 0{\cdot}206$ (P1); (f) $\mu_1 = 0{\cdot}136$ (P3); (g) $\mu_1 = 0{\cdot}205$ (chaos).

for the logistic map. This means that when the non-multiple frequency ratio system with period one response in the Poincaré section has 41 points, nevertheless the unique J-integral is collected by varying initial conditions. As long as J-integral is versus the parameter to be plotted, the response can be shown exactly.

The bifurcation of displacement versus the forcing amplitude for this winding wire system with the same parameters is shown in Figure 9, in which the periodic, quasi-periodic and chaotic motions cannot be distinguished. When a system has two frequencies with a non-multiple ratio in the Poincaré section, it may consist of a finite number of points. For systems determined by initial conditions, both the solutions of the displacement and the

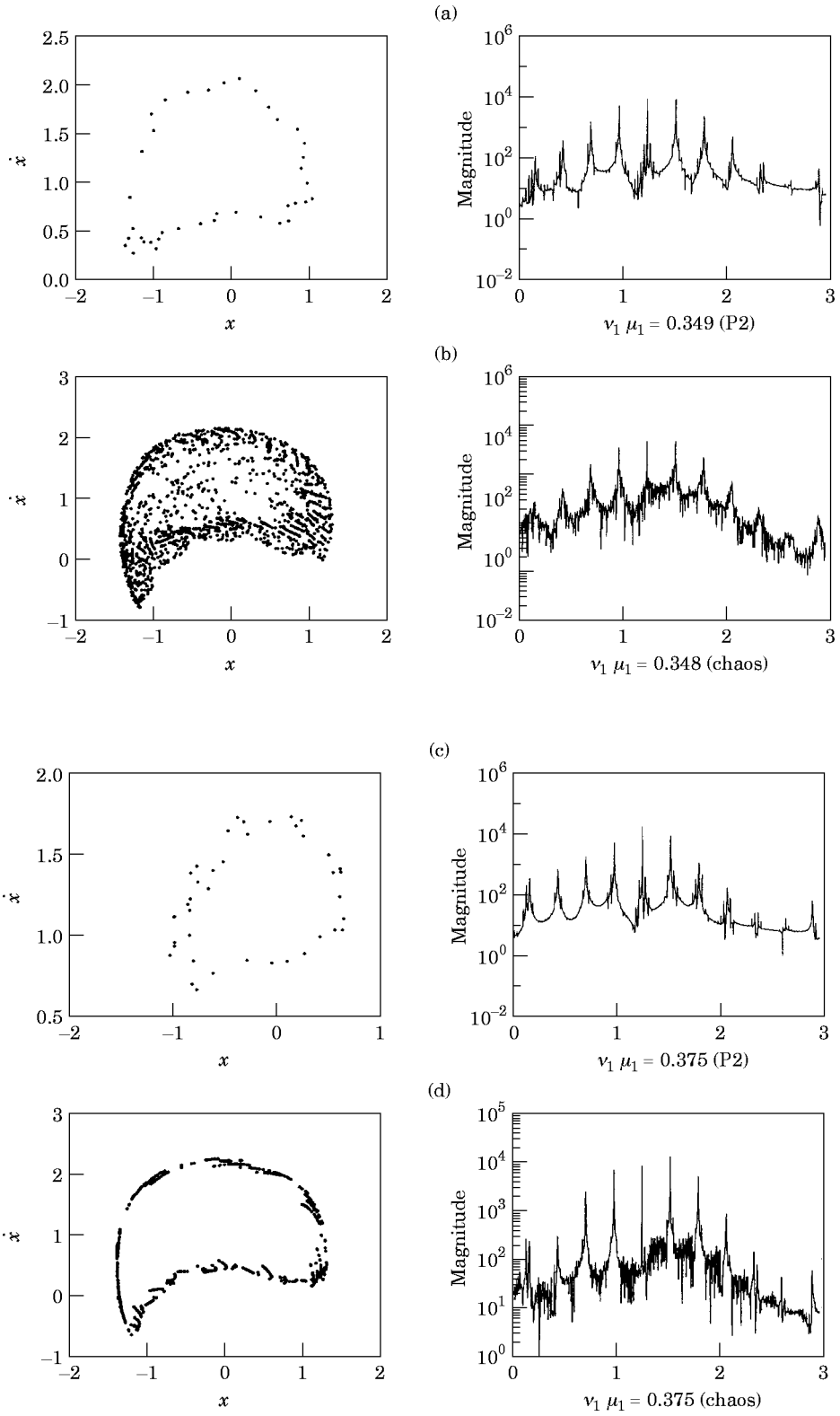
(a)
$\dot{x}$
x
Magnitude
$\nu_1\ \mu_1 = 0.349$ (P2)
(b)
$\nu_1\ \mu_1 = 0.348$ (chaos)
(c)
$\nu_1\ \mu_1 = 0.375$ (P2)
(d)
$\nu_1\ \mu_1 = 0.375$ (chaos)

Figure 7a-d.

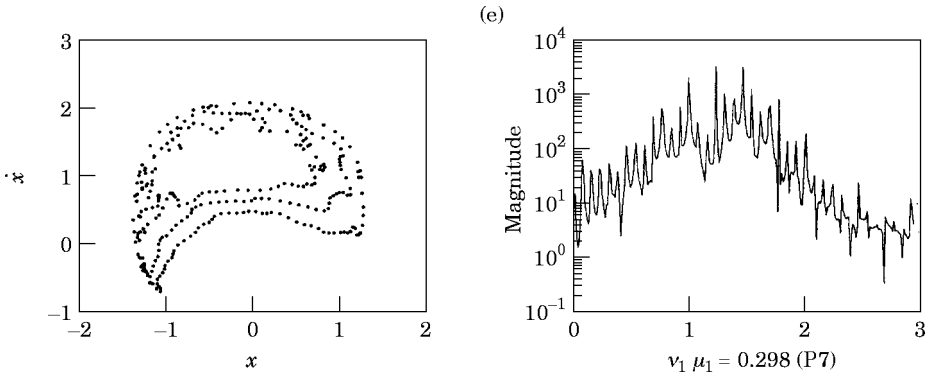

Figure 7e.

Figure 7. Poincaré maps (left) and frequency spectra (right). (a) $\mu_1 = 0{\cdot}349$ (P2); (b) $\mu_1 = 0{\cdot}348$ (chaos); (c) $\mu_1 = 0{\cdot}375$, $x(0) = -2{\cdot}1$ (P2); (d) $\mu_1 = 0{\cdot}375$, $x(0) = -2{\cdot}45$ (chaos); (e) $\mu_1 = 0{\cdot}298$ (P7).

Poincaré maps are no longer unambiguous. Thus, the bifurcation of displacement cannot give a distinct illustration of these complex oscillations.

5. STROBOSCOPE PHASE PLANE ANALYSIS

With the consideration of the J-integral, the numerical integration of this winding wire system with various initial conditions can be determined. When a transient solution of the J-integral leads to a steady state response, the system has multiple solution regions which are sensitive to the initial conditions. The large J-integrals due to resonant oscillations and the small J-integrals due to non-resonant oscillations can be obtained. For a system with various initial conditions, a number of J-integrals on the resonance cascade corresponding to period n motions can be obtained.

The resonance and non-resonance regions are determined by the two cascades of J-integrals for the domain of initial conditions of a system with specific parameters. The computational grid is divided by 101×101 for the initial conditions of $x(0) = -2{\cdot}5$ to $2{\cdot}5$ and $\dot{x}(0) = -5$ to 5. For $k = 7$, $\mu_2 = 0{\cdot}17$, $\mu_1 = 0{\cdot}25$ and $\nu_1 = 1{\cdot}23$, the phase trajectories for damping values of $\gamma = 0{\cdot}15$, $0{\cdot}1$ and $0{\cdot}07$ are shown in Figures 10(a)–10(c). In these figures the non-resonance regions are indicated by a dot, and the resonance regions, divided by a separatrix, have no sign. It can be noticed that in the vicinity of $x(0) = \dot{x}(0) = 0$ there are small J-integrals of period one motion in all cases, and that resonance regions are unsymmetric with respect to the axis $x(0) = 0$ or the axis line $\dot{x}(0) = 0$. Also, these figures show that the resonant region increases as the damping coefficient decreases. It is also desirable to determine the changes in the phase trajectory for the variations in other parameters to clarify the existence of the resonance and the non-resonance regions. In Figure 11 is shown the J-integral versus the forcing amplitude μ_1, in which the period-doubling cascades lead to chaotic motions from both directions of decreasing and increasing μ_1. Quasi-periodic and chaotic motions exist within a range of $0{\cdot}218 < \mu_1 < 0{\cdot}320$. For a narrow range around $\mu_1 = 0{\cdot}145$ irregular points occur; all possible motions contain period one motion due to resonance (large J), non-resonance (small J) and period three motion. The corresponding initial conditions can be separated/demarcated into three regions, as shown in Figure 12, denoted by blank space, dots and symbols '$\bigcirc$'. The regions of period three exist at the boundaries of both regions of resonance and non-resonance.

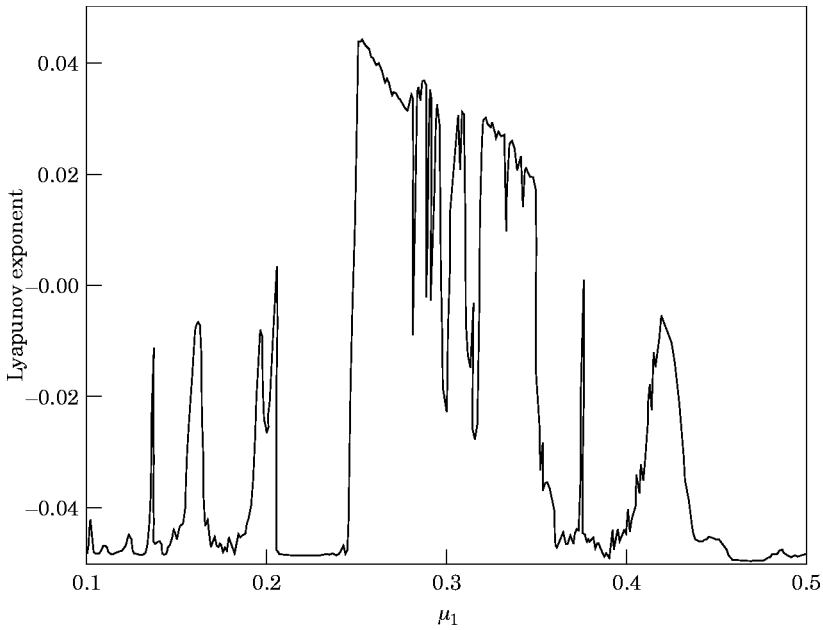

Figure 8. Lyapunov exponents versus μ_1 from Figure 5; $k = 7$, $\mu_2 = 0{\cdot}18$, $\gamma = 1/15$, $\nu_1 = 1{\cdot}23$.

6. CONCLUSIONS

The oscillations of a strongly non-linear winding wire system with two harmonic frequencies of forcing and parametric excitations have been investigated. The J-integral is utilized to determine the bifurcations of resonance and non-resonance. Period-doubling

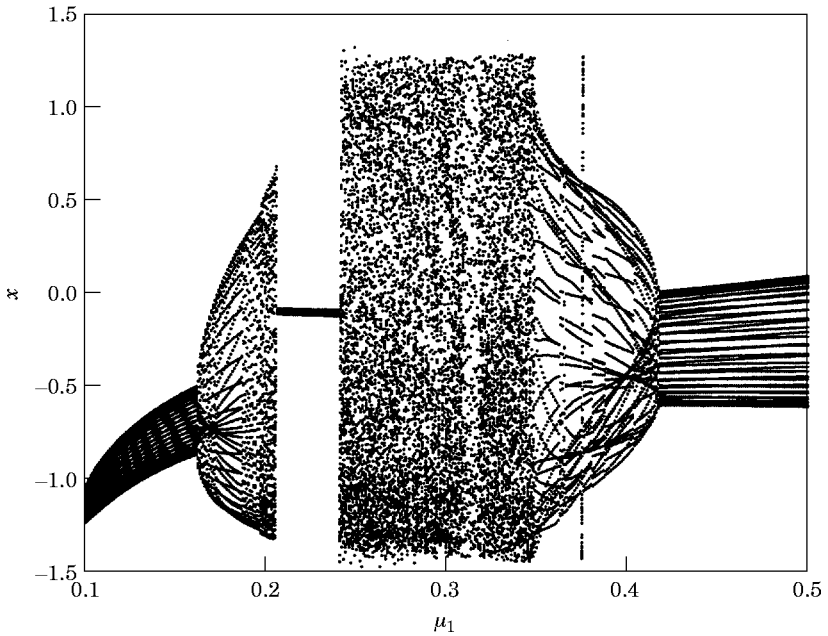

Figure 9. Bifurcation of the displacement (x–μ_1) from Figure 5.

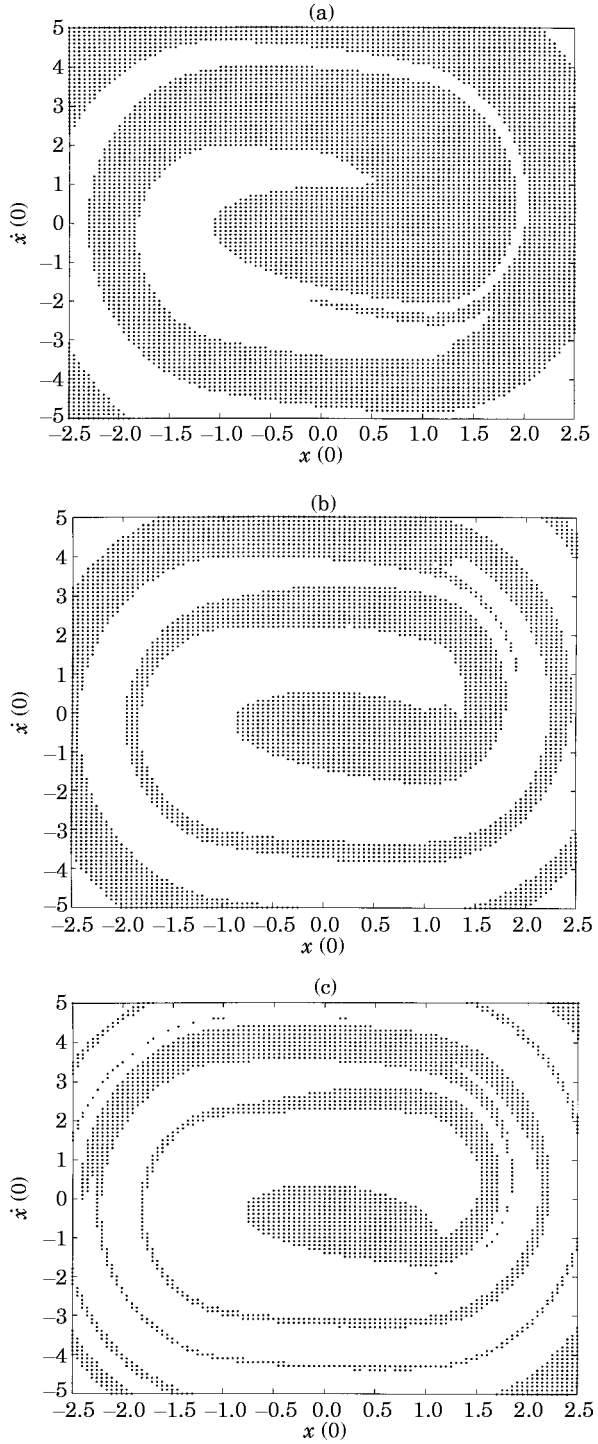

Figure 10. Resonance (blank) and non-resonance (dotted) regions from Figure 4. (a) $\gamma = 0{\cdot}15$; (b) $\gamma = 0{\cdot}1$; (c) $\gamma = 0{\cdot}07$.

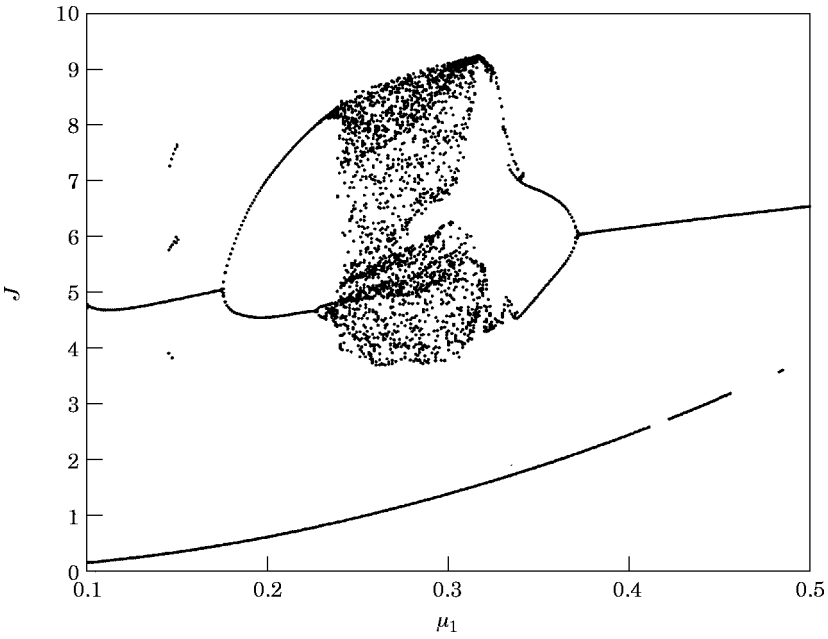

Figure 11. Bifurcation of the integral J (J–μ_1); $k = 7$, $\mu_2 = 0{\cdot}15$, $\gamma = 1/15$, $\nu_1 = 1{\cdot}23$.

and period-doubling intermittency routes to chaos have been obtained as some parameters of this system are changed.

The bifurcation of this integral exhibits a jump phenomenon in which small and large J-integrals may occur. Moreover, one may distinguish components of the resonant or non-resonant motion by the number of J-integrals with the assistance of response

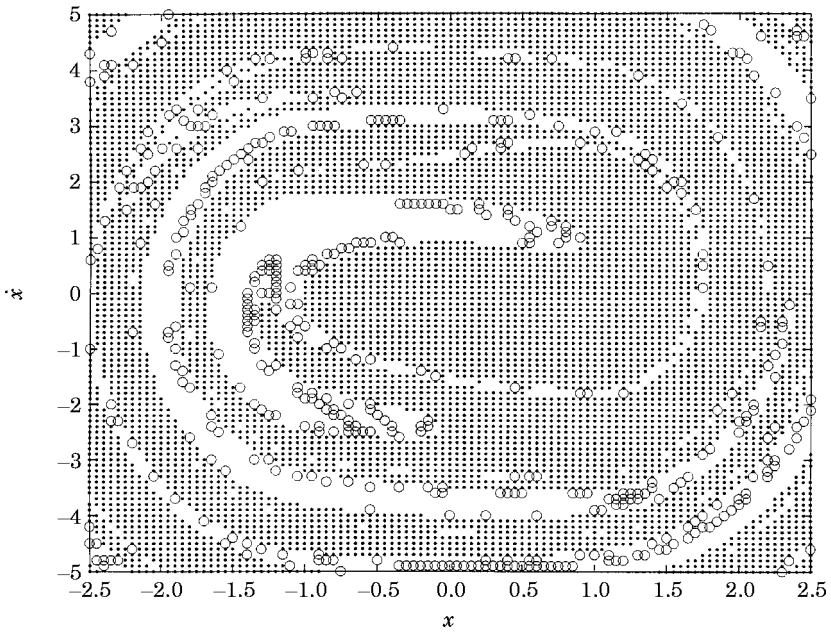

Figure 12. Resonance regions (○, P3; P1, blank) and non-resonance regions (dotted) from Figure 11 as $\mu_1 = 0{\cdot}145$.

waveforms, frequency spectra, phase portraits, Poincaré maps and Lyapunov exponents. For various parameters of this piecewise-linear system, jump phenomena, subharmonics of various orders, frequency-locked period n motion, period-doubling and period-doubling intermittency bifurcations to chaos can be observed. Also, this study established the domains of the initial conditions which lead to different stationary conditions, including resonance and non-resonance.

ACKNOWLEDGMENT

This study was supported by the National Science Council of the Republic of China, under grant number NSC 84-2212-E033-013.

REFERENCES

1. C. Padmanabhan and R. Singh 1995 *Journal of Sound and Vibration* **184**, 35–58. Analysis of periodically excited non-linear systems by a parametric continuation technique.
2. Y. S. Choi and S. T. Noah 1988 *Journal of Sound and Vibration* **121**, 117–126. Forced periodic vibration of unsymmetric piecewise-linear systems.
3. S. K. Choi and S. T. Noah 1992 *Nonlinear Dynamics* **3**, 105–121. Response and stability analysis of piecewise-linear oscillations under multi-forcing frequencies.
4. Y. B. Kim and S. T. Noah 1991 *Transactions of the American Society of Mechanical Engineers, Journal of Applied Mechanics* **58**, 545–553. Stability and bifurcation analysis of oscillators with piece-wise linear characteristics: a general approach.
5. S. L. Lau and W. S. Zhang 1992 *Transactions of the American Society of Mechanical Engineers, Journal of Applied Mechanics* **59**, 153–160. Nonlinear vibrations of piecewise-linear systems by incremental harmonic balance method.
6. S. Narayanan and P. Sekar 1995 *Journal of Sound and Vibration* **184**, 281–298. Periodic and chaotic responses of an SDF system with piecewise linear stiffness subjected to combined harmonic and flow induced excitations.
7. I. A. Mahfouz and F. Badrakhan 1990 *Journal of Sound and Vibration* **143**, 255–288. Chaotic behaviour of some piecewise-linear systems, part I: systems with set-up spring or with unsymmetric elasticity.
8. I. A. Mahfouz and F. Badrakhan 1990 *Journal of Sound and Vibration* **143**, 289–328. Chaotic behaviour of some piecewise-linear system, part II: systems with clearance.
9. A. Oks, S. Yano, S. Tsyfanskii and T. Iwatsubo 1993 *Japan Society of Mechanical Engineers International Journal, Series C* **36**, 45–51. Suppression phenomena of resonant oscillations in strongly nonlinear systems due to additional asynchronous excitations.
10. A. Wolf, J. B. Swift, H. L. Swinney and J. A. Vastano 1985 *Physica D* **16**, 285–317. Determining Lyapunov exponents from a time series.
11. T. Kapitaniak 1987 *Journal of Sound and Vibration* **114**, 588–592. Quantifying chaos with amplitude probability density function.
12. T. Kapitaniak 1988 *Journal of Sound and Vibration* **121**, 259–268. Combined bifurcation and transition to chaos in a non-linear oscillator with two external periodic.
13. G. Schmidt and A. Tondl 1986 *Non-linear Vibration*. New York: Cambridge University Press.
14. R. C. Hilborn 1994 *Chaos and Nonlinear Dynamics*. Oxford: Oxford University Press.

APPENDIX: NOMENCLATURE

c	damping coefficient
e	eccentricity
f_p	frequency spectrum of the peak frequencies
J	$= \int_0^{2\pi/\nu_1} [\dot{x}(\tau)]^2 \, d\tau$, integral monitored
k	$= (k_2 - k_1)/k_1$, non-dimensional stiffness
k_1	winding stiffness
k_2	suppression stiffness
m	lump mass of a winding wire

n, n_1, n_2	integers
p	amplitude of forcing excitation
Pn	period n motion with nth order subharmonic frequencies
t	time
T	$= 2\pi/v_1$, forcing period
x	$= y/\varepsilon$, non-dimensional displacement
y	lateral displacement of SDOF wire
γ	$= c/(m\omega_0)$, non-dimensional damping coefficient
$\Delta\omega_n$	$= \lvert v_2 - 2v_1 \rvert/n$
ε	clearance
μ_1	$= p/(k_1\,\varepsilon)$, non-dimensional amplitude of forcing excitation
μ_2	non-dimensional amplitude of parametric excitation
v_1	$= \omega_1/\omega_0$, non-dimensional forcing frequency
v_2	$= \omega_2/\omega_0$, non-dimensional parametric frequency
τ	$= \omega_0\,t$, non-dimensional time
ω_0	$= \sqrt{k_1/m}$, fundamental natural frequency of the linearized wire system
ω_1	forcing frequency
ω_2	parametric frequency